Surface Chemistry

DOI: 10.1002/anie.201200773

Flexible Nanogenerators Based on Graphene Oxide Films for Acoustic Energy Harvesting**

Ronghui Que, Qi Shao, Qinliang Li, Mingwang Shao, Shiduan Cai, Suidong Wang,* and Shuit-Tong Lee**

Harvesting ubiquitous mechanical energy, an important energy resource, directly from the environment has been proposed as an effective approach to powering nanodevices.[1,2] Numerous piezoelectric nanogenerators, such as zinc oxide (ZnO) nanowires,[3] indium nitride (InN) nanowires,[4] lead zirconate titanate nanofibers,[5] poly(vinylidene fluoride) nanofibers,[6] and cadmium sulfide (CdS) nanowires[7] have been explored for converting mechanical energy into electricity. For practical applications, low-cost, high-efficiency nanogenerators are demanded that can be fabricated on flexible substrates and require only simple integration processes.

Graphene oxide (GO), a derivative of graphene, consists of a hexagonal ring of carbon network having both sp^2- and sp^3-hybridized carbon atoms bearing hydroxyl and epoxide functional groups on basal planes, as well as carbonyl and carboxyl groups at the edges of the sheet.[8,9] Those functional groups can extensively modify the electronic structure and chemical properties of GO,[10–12] enabling various applications.[14–24] Here, we report the exciting application of GO as a flexible, high-efficiency nanogenerator, realized through oxygen-containing functional groups which enable GO to store charges and harvest acoustic energy.

In this study, GO exfoliated from a modified Hummer method[13,14] was used to fabricate a nanogenerator, which could convert acoustic energy to electricity at a high conversion efficiency of 12.1%. The induced mean current is sensitively dependent on the pH values of the suspensions used to prepare the GO films. The findings reveal the exciting potential of GO for fabricating nanogenerators for energy harvesting, as well as a novel avenue for nanoelectronic applications.

GO was synthesized from expandable graphitic flakes using the modified Hummer method.[13,14] Graphene was purchased from Sigma–Aldrich and used as received. The crystal structure of the samples was characterized with transmission electron microscopy (TEM, FEI Tecnai F20, 200 kV). Raman spectra were recorded using a confocal microprobe Raman system (HR800, Jobin Yvon) using a 633 nm HeNe laser. The electronic structure of carbon was characterized with X-ray photoemission spectroscopy (XPS, Kratos Axis UltraDLD, monochromatized Al K_α source) operated at a base pressure of 5×10^{-10} Torr. Atomic force microscopy (AFM) measurements were conducted with a Mutilmode V AFM system (Veeco). All the experimental processes are listed in the Supporting Information.

The as-prepared GO suspensions from different pH solutions (adjusted with HCl and NaOH) and different concentrations were dropped onto a Teflon tape, followed by drying in a convection oven at 60 °C for 30 min to form GO films. The morphology of the GO films was characterized by scanning electron microscopy (SEM) with a FEI Quanta 200F SEM spectrometer. Microattenuated total-reflection (ATR)-Fourier transform infrared (FTIR) measurements were performed in air using a Bruker FTIR spectrometer.

The low-magnification TEM image (Figure 1 a) shows few layers of GO sheets with many wrinkled and folded regions. The selected-area electron diffraction (SAED) pattern from the GO layers (inset of Figure 1 a) reveals that the original graphene lattice is present.[24]

The characteristic Raman G peak at around 1580 cm^{-1} in graphene (curve 1, Figure 1 b) is obviously broadened and blue-shifted relative to that at around 1597 cm^{-1} in GO (curve 2, Figure 1 b), indicating higher disorder in the latter, which is also supported by the broadened D band (1335 cm^{-1}) of GO relative to that of graphene.[25] The D peak (Figure 1 b) is strong in GO suggesting a high level of disorder.[26] The intensity ratio of the D and G peaks increases sharply from 0.1 in graphene to 1.1 in GO, reflecting the decrease of in-plane sp^2 domain size and the increase of structure disorder in the GO sheets.

XPS was performed to quantify the oxygen-containing groups. The C 1s spectrum in Figure 1 c clearly indicates a considerable degree of oxidation with four components: 26.58% alcohols or ethers (286.3 eV), 21.49% carboxyl (C=O) groups (287.3 eV), and 10.36% carboxyl (COOH) or ester (COOR) groups (288.6 eV).[27,28] Those results are consistent

[*] Dr. R. Que, Q. Shao, Q. Li, Prof. M. Shao, S. Cai, S. Wang
Jiangsu Key Laboratory for Carbon-Based Functional Materials & Devices, Institute of Functional Nano & Soft Materials
Soochow University, Suzhou, Jiangsu, 215123 (China)
E-mail: mwshao@suda.edu.cn
wangsd@suda.edu.cn
Prof. S.-T. Lee
Center of Super-Diamond and Advanced Films (COSDAF) and Department of Physics and Materials Science
City University of Hong Kong, Hong Kong SAR (China)
E-mail: apannale@cityu.edu.hk

[**] This work was supported by the National Natural Science Foundation of China (grant numbers 21071106 and 51072126), the research grants council of HKSAR (grant number CityU5/CRF/08), the NSFC-RGC joint scheme (grant number N_CityU 108/08), the National Basic Research Program of China (973 Program; grant number 2012CB932903), and a project funded by the priority academic program development of Jiangsu Higher Education Institutions.

Supporting information for this article is available on the WWW under http://dx.doi.org/10.1002/anie.201200773.

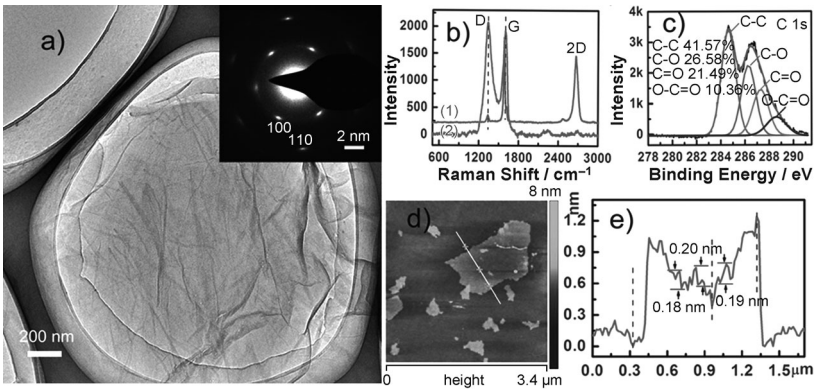

Figure 1. a) Structure and morphology of the GO sample: TEM image and SAED pattern (inset). b) Raman spectra of GO (curve 2) and graphene (curve 1). c) C 1s XPS spectrum of GO and the four C components from the fitted curves. d) AFM of the GO. e) The section analysis corresponding to (d).

with the corresponding oxygen contents used for the fit function in the Figure S1 (Supporting Information), demonstrating a large fraction of oxygen in GO.

The AFM image in Figure 1 d reveals the presence of irregularly shaped sheets with lateral dimension ranging from a few hundred nanometer to a few micrometer. The typical section analyses in Figure 1 e and Figure S2 (see the Supporting Information) show the existence of the monolayer graphene and the presence of isolated epoxy and hydroxyl reaction sites according to previous reports[29] (detailed discussions are listed in the Supporting Information).

Figure 2 a sketches the fabrication process of the GO film device. The GO film shown in Figure S4 (see the Supporting Information) was made from 100 μL GO suspension (2 g L^{-1}) at pH 5. The thickness of the film is around 50 μm and the diameter is around 5.8 mm. Remarkably, the GO film exhibited great repulsion to a glass rod which had been rubbed against silk, and slight attraction to a rubber rod rubbed against fur. This phenomenon indicated that the GO film was positively charged, which was different from the GO sheets in suspensions (Figure S5 in the Supporting Information) in which the negative zeta potentials showed a similar trend as previously reported.[30,31] The origin of the positively charged GO films was that: 1) H^+ can either be stored in quantized levels of nanosized graphene, or trapped in the amorphous regions on the GO dielectric where oxygen functionalities have a high electron affinity;[32] 2) the protonation of the carboxylate groups could directly result in the delocalization of positive charges.[33,34] And the reason for the negative zeta potential is that numerous H^+ ions entered the GO and a large number of OH^- ions adsorbed in the shear plane, which caused a reverse electricity of the zeta potential.

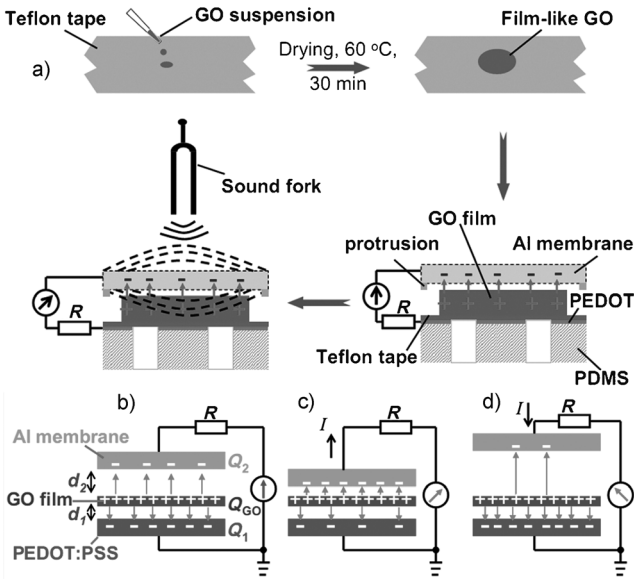

Figure 2. a) Schematic of the device fabrication. b–d) The equivalent circuit of current generation.

The charged film could be assembled into an energy harvester as shown in Figure 2 a. This structure consisted of only one movable part, which may yield sustainable and stable output currents.[35] The detailed fabrication of the energy harvesting nanogenerator is described in the Supporting Information.

The circuit scheme of the GO-based nanogenerator is shown in Figure 2 b–d, where the GO film is attached to the bottom poly(3,4-ethylenedioxythiophene) poly(styrenesulfonate), PEDOT:PSS, electrode with the insulation of Teflon tape on one side, and is covered by the top Al membrane with the insulation of protrusion on the other side. As the charges are confined in the GO film, the total positive charge quantity ($Q_{GO} \approx 20$ pC cm^{-2} in the present case) is fixed. As both the electrodes are grounded, Q_{GO} is screened by the induced negative charges both in the PEDOT:PSS electrode (with quantity of Q_1) and in the Al membrane (with quantity of Q_2), which follow $Q_{GO} = Q_1 + Q_2$. In this case, the device can be regarded as two flat-panel capacitors in parallel with capacitances of $C_1 = \varepsilon_1 S/d_1$ and $C_2 = \varepsilon_2 S/d_2$, where C_1, ε_1, and d_1 are the capacitance of the bottom capacitor, the dielectric constant of the Teflon tape, and the distance between the GO film and the PEDOT:PSS electrode, respectively; C_2, ε_2, and d_2 are the capacitance of the top capacitor, the dielectric constant of air, and the distance between the GO film and the Al membrane, respectively; and S is the surface area of the GO film. As d_1 is fixed, C_1 is unchanged. On the other hand, C_2 is variable as d_2 can be changed by the Al membrane vibration. Considering $Q_1 = C_1 V_{GO}$ and $Q_2 = C_2 V_{GO}$, where V_{GO} is the electric potential of the GO film, from the above equations Q_1 and Q_2 can be expressed as Equations (1) and (2):

$$Q_1 = \frac{C_1 Q_{GO}}{C_1 + C_2} = \frac{\varepsilon_1 d_2 Q_{GO}}{\varepsilon_1 d_2 + \varepsilon_2 d_1} \quad (1)$$

$$Q_2 = \frac{C_2 Q_{GO}}{C_1 + C_2} = \frac{\varepsilon_2 d_1 Q_{GO}}{\varepsilon_1 d_2 + \varepsilon_2 d_1} \quad Q_2 = \frac{C_2 Q_{GO}}{C_1 + C_2} = \frac{\varepsilon_2 d_1 Q_{GO}}{\varepsilon_1 d_2 + \varepsilon_2 d_1}. \quad (2)$$

When the sound fork is stationary, the Al membrane remains steady (Figure 2b) so that Q_1 and Q_2 are unchanged, and thus only the background noise current (around 2.9 pA) can be detected in the circuit. When the sound fork is vibrating, the Al membrane could responsively vibrate, and the changes in d_2 and hence in C_2 would follow. Consequently, altering d_2 would cause the charge redistribution in Q_1 and Q_2 according to Equations (1) and (2). For instance, when Q_1 is increased by ΔQ, Q_2 will be decreased by ΔQ correspondingly; and vice versa. Therefore, both the increase and decrease in d_2 induced by the vibration of the Al membrane can result in a transient current as schematically depicted in Figure 2c,d, respectively. Based on this mechanism, acoustic energy can be absorbed by the GO-based nanogenerator and a continuous alternating current could be generated in the circuit, as demonstrated in Figure 3 and in Figure S6 (see the Supporting Information).

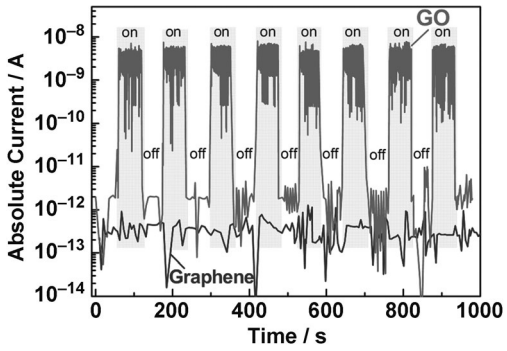

Figure 3. Current of GO/graphene nanogenerator versus sound fork vibration.

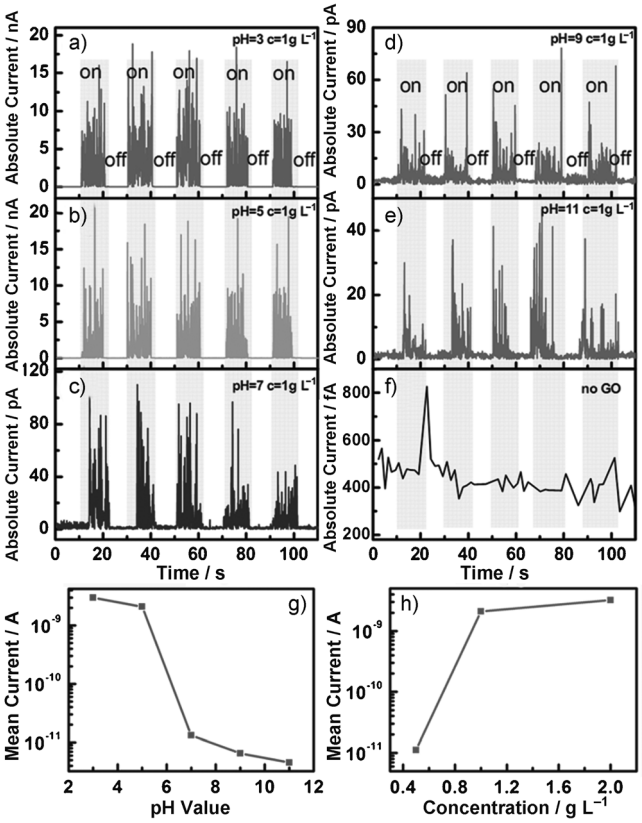

Figure 4. Current of GO nanogenerators from different pH suspension: a) 3, b) 5, c) 7, d) 9, and e) 11, respectively, versus the sound fork vibrations. The GO concentration is 1 g L^{-1}. f) Current of a nanogenerator with no GO film versus the sound fork vibrations. g) Output mean current versus pH values. h) Output mean current versus the GO concentration.

The average absolute current is about 3.23 nA (see Figure S6 in the Supporting Information) with a large signal-to-noise ratio of over 1000. In contrast, no current response was observed in the device made of graphene (Figure 3) or in the reference device without GO (Figure 4f) using the identical device structure, indicating that the charged GO film was responsible for the current generation in Figure 3. The simple GO-based device can indeed be served as a flexible nanogenerator for conversion of acoustic to electrical energy, and note that this nanogenerator can work no matter if the GO film is positively or negatively charged.

The efficiency of the electrical power generated by the GO device is calculated as follows: the output electrical power from the device is $IV_0 = 4.24 \times 10^{-10}$ W, where I is the average current in Figure 3 and Figure S5, and $V_0 = Q_0/C$ with Q_0 and C determined by the simple plot in Figure S7 (see the Supporting Information). The acoustic energy generated by the fork is determined by a sound level meter. Taking into account the receiving area in the present experimental design, the input sound power to the device is 3.51×10^{-9} W. Therefore, the conversion efficiency of acoustic to electrical energy is $4.24 \times 10^{-10}/(3.51 \times 10^{-9}) = 12.1\,\%$ (see the Supporting Information).

The GO-based nanogenerator is extremely attractive because of the unique structure and properties, such as low cost and facile processing of GO films, controllability of oxidation level, and device simplicity and flexibility, which are desirable features for acoustic energy harvesting.

To evaluate the effect of the $[H^+]$ concentration on the current generation, a series of nanogenerators were fabricated using GO suspensions (1 g L^{-1}) with different pH values (3, 5, 7, 9, and 11). Figure 4 compares the vibration response of the GO films made from GO suspensions with different $[H^+]$ concentration. The nanogenerators made from pH 3 and pH 5 suspensions responded violently to fork vibrations, generating large currents of 3.0 and 2.1 nA, respectively (Figure 4a,b), which suggested the GO films made from low pH suspensions had a huge amount of charges. In contrast, the mean current generated from the nanogenerators made from pH 7, 9 and 11 suspensions are much smaller. The variation of mean current in the pH range of 3–11 was larger than 10^2 (Figure 4c–e), indicating that the GO films made from high pH suspensions contained fewer charges. Figure 4g illustrates the correlation between the pH values and the output mean currents. The results demonstrate that the $[H^+]$ concentration indeed affects the amount of charges on the GO films, and is critical for current generation.

Keeping the pH value (=5) constant, the current (I) to voltage (V) characteristics of a series of nanogenerators made from GO suspensions with different GO concentrations were

measured. As shown in Figure S8 (see the Supporting Information), the nanogenerators showed different responses to acoustic energy. The GO film made from a high GO concentration generated a relatively large mean current because of the large total amount of charges (Figure S6 in the Supporting Information). In contrast, the nanogenerator made from low GO concentration responded weakly and produced a small current (see Figure S8b in the Supporting Information). The proportional relationship between GO concentration and mean generated current (Figure 4h) shows that the GO concentration is another key parameter in determining the nanogenerator performance.

In GO suspensions with low pH value, H^+ will be readily trapped by the oxygen functionalities, especially the epoxy functionality on the GO sheets.[32,36] Consequently, the protonated oxygen-containing functional groups render the GO films positively charged, and the amount of charges is associated with the $[H^+]$ concentration.

To further elucidate the effect of $[H^+]$ concentration, attenuated total reflectance (ATR) FTIR spectroscopy, was employed to measure functional groups attached to carbon materials[37] and to monitor the GO film surfaces made from different pH suspensions. Figure 5a shows the normalized ATR-FTIR spectrum of the GO films made from pH 3, 5, 7, 9, and 11, respectively. The band located at 1720 cm^{-1} in curves 1–4 of Figure 5a is attributed to the stretching vibration of protonated carboxyl acid because of the conjugated carboxyl groups or the formation of hydrogen bonds between -COOH and epoxy groups.[38,39] The decreasing absorption is indicative of a decreasing carboxyl acid stretching mode with increasing pH value, which is accompanied by a significant increase in intensity of the 1667 cm^{-1} band at pH 11 (curve 5 in Figure 5a), which is assigned to the antisymmetric stretching mode of $-COO^-$.[41,42] Of particular interest is that the relative intensities of the bands at 740, 780, 870, and 981 cm^{-1}, because of epoxy vibrations,[42] increases at first, then almost monotonously decreases with increasing pH value, indicating that the amount of epoxy functionalities on the GO sheets gradually diminishes. Meanwhile, the vibrations of C–O located at around 1126 and 1280 cm^{-1},[37,39] become more obvious in the GO films made from higher pH (curves 4 and 5, Figure 5a), suggesting that the abundance of C–O content increases along with increasing pH value. The band at 1440 cm^{-1} may have contributions from both C–O stretching and O–H bending modes in carboxylic acid groups[38] and decreases greatly at pH 11, showing the rapid decline of O–H content because of the formation of sodium salts.

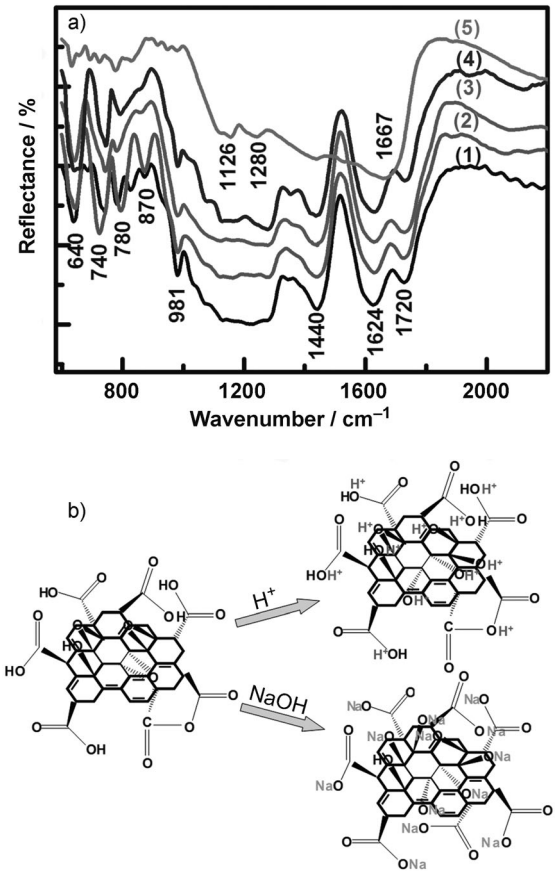

Figure 5. a) Normalized ATR-FTIR spectra of GO films from different pH values: curve 1) 3, curve 2) 5, curve 3) 7, curve 4) 9, and curve 5) 11. b) GO surfaces under low and high pH conditions.

The above discussions suggest the changes of the surface structure of GO as shown in Figure 5b. Under abundant $[H^+]$ conditions, H^+ will be trapped on the GO sheet through hydrogen bonding or oxygen, thereby forming positively charged GO films. The amount of charges would increase with increasing $[H^+]$ concentration, in agreement with the response current in Figure 4a,b. On the other hand, high pH or $[OH^-]$ conditions would lead to reaction of the epoxy and carboxyl groups with OH^- to form the sodium salts resulting in fewer hydroxyl groups to trap charges, thereby the induced current would become smaller (Figure 4d,e).

To get a more realistic circuit design, a large load (1 MΩ) was employed. The mean induced current was measured to be 2.84×10^{-9} A, showing the output power of 8.07×10^{-12} W.

In summary, GO sheets obtained from the modified Hummer method are positively charged because of H^+ charge trapping through oxygen-containing functional groups. The charged GO films can be conveniently integrated into nanogenerators for harvesting acoustic energy with a high energy conversion efficiency of 12.1%, which is strongly dependent on the $[H^+]$ and GO concentration. As the GO-based nanogenerators are low-cost, easily processed, highly efficient, and flexible, they are promising candidates for acoustic energy harvesting.

Received: January 28, 2012
Revised: March 30, 2012
Published online: April 18, 2012

Keywords: carbon · graphene oxide · nanoparticles · photothermal therapy · surface chemistry

[1] C. T. Huang, J. H. Song, W. F. Lee, Y. Ding, Z. Gao, Y. Hao, L. J. Chen, Z. L. Wang, *J. Am. Chem. Soc.* **2010**, *132*, 4766–4771.
[2] S. Xu, Y. Qin, C. Xu, Y. Wei, R. Yang, Z. L. Wang, *Nat. Nanotechnol.* **2010**, *5*, 366–373.

[3] Z. L. Wang, J. Song, *Science* **2006**, *312*, 242 – 246.
[4] C. T. Huang, J. Song, C. M. Tsai, W. F. Lee, D. H. Lien, Z. Gao, Y. Hao, L. J. Chen, Z. L. Wang, *Adv. Mater.* **2010**, *22*, 4008 – 4013.
[5] X. Chen, S. Xu, N. Yao, Y. Shi, *Nano Lett.* **2010**, *10*, 2133 – 2137.
[6] C. Chang, V. H. Tran, J. Wang, Y. K. Fuh, L. Lin, *Nano Lett.* **2010**, *10*, 726 – 731.
[7] Y. F. Lin, J. Song, Y. S. Ding, Y. Lu, Z. L. Wang, *Adv. Mater.* **2008**, *20*, 3127 – 3130.
[8] T. Szabó, O. Berkesi, P. Forgó, K. Josepovits, Y. Sanakis, D. Petridis, I. Dékány, *Chem. Mater.* **2006**, *18*, 2740 – 2749.
[9] A. Lerf, H. He, M. Forster, J. Klinowski, *J. Phys. Chem. B* **1998**, *102*, 4477 – 4482.
[10] I. Jung, D. A. Dinkin, R. D. Piner, R. S. Ruoff, *Nano Lett.* **2008**, *8*, 4283 – 4287.
[11] A. B. Kaiser, C. G. Navarro, R. S. Sundaram, M. Burghard, K. Kern, *Nano Lett.* **2009**, *9*, 1787 – 1792.
[12] G. Eda, C. Mattevi, H. Yamaguchi, H. Kim, M. Chhowalla, *J. Phys. Chem. C* **2009**, *113*, 15768 – 15771.
[13] W. S. Hummers, R. E. Offeman, *J. Am. Chem. Soc.* **1958**, *80*, 1339.
[14] Z. Liu, J. T. Robinson, X. M. Sun, H. J. Dai, *J. Am. Chem. Soc.* **2008**, *130*, 10876 – 10877.
[15] N. Mohanty, V. Berry, *Nano Lett.* **2008**, *8*, 4469 – 4476.
[16] Y. Liu, D. S. Yu, C. Zeng, Z. C. Miao, L. M. Dai, *Langmuir* **2010**, *26*, 6158 – 6160.
[17] Z. J. Wang, X. Z. Zhou, J. Zhang, F. Boey, H. Zhang, *J. Phys. Chem. C* **2009**, *113*, 14071 – 14075.
[18] C. T. Hsieh, S. M. Hsu, J. Y. Lin, H. Teng, *J. Phys. Chem. C* **2011**, *115*, 12367 – 12374.
[19] J. T. Robinson, M. Zalalutdinov, J. W. Baldwin, E. S. Snow, Z. Wei, P. Sheehan, B. H. Houston, *Nano Lett.* **2008**, *8*, 3441 – 3445.
[20] G. Eda, M. Chhowalla, *Nano Lett.* **2009**, *9*, 814 – 818.
[21] J. T. Robinson, F. K. Perkins, E. S. Snow, Z. Wei, P. E. Sheehan, *Nano Lett.* **2008**, *8*, 3137 – 3140.
[22] Q. Liu, Z. F. Liu, X. Y. Zhang, L. Y. Yang, N. Zhang, *Adv. Funct. Mater.* **2009**, *19*, 894 – 904.
[23] K. K. Manga, Y. Zhou, Y. Yan, K. P. Loh, *Adv. Funct. Mater.* **2009**, *19*, 3638 – 3643.
[24] P. P. Yao, P. L. Chen, L. Jiang, H. P. Zhao, H. F. Zhu, *Adv. Mater.* **2010**, *22*, 5008 – 5012.
[25] K. N. Kudin, B. Ozbas, H. C. Schniepp, R. K. Prud'homme, I. A. Aksay, R. Car, *Nano Lett.* **2008**, *8*, 36 – 41.
[26] G. Eda, M. Chhowalla, *Adv. Mater.* **2010**, *22*, 2392 – 2415.
[27] Y. M. Xie, P. M. A. Sherwood, *Chem. Mater.* **1990**, *2*, 293 – 299.
[28] S. D. Gardner, C. S. K. Singamsetty, G. L. Booth, G. R. He, C. U. Pittman, *Carbon* **1995**, *33*, 587 – 595.
[29] H. C. Schniepp, J. L. Li, M. J. Mcallister, H. Sai, M. H. Alonso, *J. Phys. Chem. B* **2006**, *110*, 8535 – 8539.
[30] S. A. Hasan, J. L. Rigueur, R. R. Harl, A. J. Krejci, I. Gonzalo-Juan, B. R. Rogers, J. H. Dickerson, *ACS Nano* **2010**, *4*, 7367 – 7372.
[31] D. W. Lee, T. K. Hong, D. Kang, J. Lee, M. Heo, J. Y. Kim, B. S. Kim, H. S. Shin, *J. Mater. Chem.* **2011**, *21*, 3438 – 3442.
[32] S. Wang, J. Pu, D. S. H. Chan, B. J. Cho, K. P. Loh, *Appl. Phys. Lett.* **2010**, *96*, 143109 – 3.
[33] W. Zhao, C. Song, P. E. Pehrsson, *J. Am. Chem. Soc.* **2002**, *124*, 12418 – 12419.
[34] S. Ramesh, L. M. Ericson, V. A. Davis, et al., *J. Phys. Chem. B* **2004**, *108*, 8794 – 8798.
[35] R. H. Que, M. W. Shao, S. D. Wang, D. D. D. Ma, S. T. Lee, *Nano Lett.* **2011**, *11*, 4870 – 4873.
[36] I. Y. Lee, E. S. Kannan, G. H. Kim, *Appl. Phys. Lett.* **2009**, *95*, 263308 – 363310.
[37] H. Peng, L. B. Alemany, J. L. Margrave, V. N. Khabashesku, *J. Am. Chem. Soc.* **2003**, *125*, 15174 – 15182.
[38] Y. F. Jia, K. M. Thomas, *Langmuir* **2000**, *16*, 1114 – 1122.
[39] J. D. Kubicki, L. M. Schroeter, M. J. Itoh, B. N. Nguyen, S. E. Apitz, *Geochim. Cosmochim. Acta* **1999**, *63*, 2709 – 2725.
[40] E. Nabedryk, J. Breton, R. Hienerwadel, C. Fogel, W. Maentele, M. L. Paddock, M. Y. Okamura, *Biochemistry* **1995**, *34*, 14722 – 14732.
[41] J. Zhang, H. Zou, Q. Qing, Y. Yang, Q. Li, Z. F. Liu, X. Guo, Z. Du, *J. Phys. Chem. B* **2003**, *107*, 3712 – 3718.
[42] J. G. Speight, *Lange's handbook of chemistry*, McGraw-Hill, New York, **1972**.

